

CONFERENCES AND SYMPOSIA

PACS numbers: 72.25.Hg, **74.78. – w, 74.45. + c**

90th ANNIVERSARY OF THE P.L. KAPITZA INSTITUTE FOR PHYSICAL PROBLEMS, RUSSIAN ACADEMY OF SCIENCES

Josephson π-junctions and Andreev current-transport 'engineering' in S–N/F–S nanostructures *

V.V. Ryazanov, T.E. Golikova, V.V. Bol'ginov, I.V. Bobkova, A.M. Bobkov

DOI: https://doi.org/10.3367/UFNe.2024.12.039922

Contents

Abstract. We present a review of studies of two types of Josephson π-junctions, i.e., Josephson structures with an inverse current–phase relation. In particular, we discuss the features of the transition to the π-state of Josephson superconductor–ferromagnet–superconductor sandwiches (Josephson SFS junctions). At the same time, much attention is devoted to the 'Andreev' coherent transport in planar superconductor–normal metal–superconductor structures (Josephson SNS junctions) and transitions to the π-state caused by a nonequilibrium electron distribution in a Josephson junction with a normal metal barrier. We also discuss in detail various types of nonequilibrium distributions arising in hybrid Josephson S–N/F–S structures upon injection of spin-polarized carriers into the Josephson barrier and the features of Andreev current transport due to contacts between a normal metal and a ferromagnet in the Josephson barrier. The review relies mainly on the works performed with the participation of the authors.

Keywords: superconductivity, Josephson effect, inverse phase difference across junctions, π-junctions, Josephson barriers with nonequilibrium electron distribution

V.V. Ryazanov [1, 2, *], **T.E. Golikova** [1], **V.V. Bol'ginov** [1], **I.V. Bobkova** [2], **A.M. Bobkov** [2]
[1] Institute of Solid State Physics, Russian Academy of Sciences, ul. Akademika Osip'yana 2, 142432 Chernogolovka, Moscow region, Russian Federation
[2] Moscow Institute of Physics and Technology (National Research University), Institutskii per. 9, 141701 Dolgoprudny, Moscow region, Russian Federation
E-mail: [*] valery.ryazanov@gmail.com

Received 18 December 2024
Uspekhi Fizicheskikh Nauk **195** (7) 766 – 777 (2025)
Translated by I.A. Ulitkin

1. Introduction

Among the promising areas of development for fundamentally new types of electronics in a 'post-silicon' future, superconducting electronics stands out for its advantages related to high speed, energy efficiency, ability to implement quantum coherent structures (qubits), etc. Josephson ('tunnel') junctions, in which, along with a thin dielectric layer, normal metals and ferromagnets are used as barriers, are versatile components of superconducting electronics. Josephson superconductor–normal metal–superconductor (SNS) junctions enable coherent (superconducting) current transport by means of 'Andreev reflection' at the NS interfaces of such junctions. Andreev reflection at the interface between a normal metal and a superconductor is a remarkably beautiful phenomenon, first described by A.F. Andreev in 1964. [1]. Coherent current is transported across the NS interface due to reflection (conversion) of an electron into a hole in the normal metal (or, conversely, a hole into an electron) and the appearance (disappearance) of a single Cooper pair with a charge of $2e$ in the superconductor. In a Josephson SNS junction, there are two NS interfaces, and the carriers reflected from them (electron to hole and then back to electron) represent a bound 'Andreev' electron-hole pair trapped in a potential well in the Josephson N-layer sandwiched between two superconductors. This leads to the appearance of discrete 'Andreev' levels, which provide superconducting current transport through the normal-metal barrier [2]. The relation between the superconducting current

[*] Joint meeting of the Scientific Session of the Physical Sciences Division of the Russian Academy of Sciences and the Scientific Council of the Kapitza Institute for Physical Problems of the Russian Academy of Sciences, dedicated to the 90th anniversary of the Kapitza Institute for Physical Problems, Russian Academy of Sciences (December 18, 2024) (see *Phys. Usp.* **68** (7) 699 (2025); *Usp. Fiz. Nauk* **195** (7) 747 (2025)).

I_S and the phase difference ϕ of the superconducting wave function in the Josephson junction is 2π-periodic (in the simplest case, $I_S = I_c \sin\phi$); i.e., the superconducting current changes sign when the phase difference $\phi = \pi$ is reached at the junction (the relation $I_S = I_c \sin\phi$ changes to $I_S = I_c \sin(\phi + \pi) = -I_c \sin\phi$). Therefore, Andreev levels must arise in pairs, one of which carries current in the direction set by the current source connected to the Josephson junction, and the neighboring (higher energy) level carries current in the opposite direction. The current-phase relation for the SNS junction and the Andreev states in the N barrier in the diffusive limit will be discussed in more detail in the following sections.

In 1999, Baselmans et al. [3] performed an experiment in which the nonequilibrium electron distribution in the N barrier, established by the voltage across the N layer, transferred the SNS junction to a higher energy level, which carries the current of the opposite direction, corresponding to a shift in the current-phase relation by π, i.e., corresponding to the π-state. In 2001, with the participation of a co-author of this review, another π-junction was also implemented based on a Josephson junction with a ferromagnetic layer as a barrier (SFS junction) [4–7]. In this junction, the inversion of the current-phase relation was stipulated by the appearance, under the action of an exchange field, of a nonzero total momentum of a Cooper pair passing through the F layer, which leads to a phase shift π at the SFS junction.

The above approaches were combined in a series of studies involving the authors of this review [8, 9]. The implementation of planar submicron S–N/F–S junctions with a ferromagnetic sublayer in the Josephson N-barrier region made it possible to produce induced spin polarization in the barrier and significantly change the coherent Andreev current transport through the N layer. This review is devoted to a discussion of the obtained results and a theoretical description of the structure of states that carry the superconducting current in such junctions.

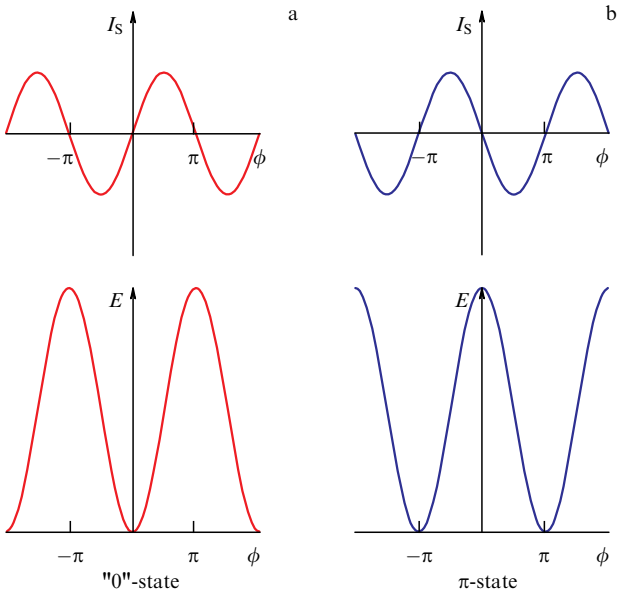

Figure 1. Dependence of superconducting current I_S and coupling energy E on phase difference for a Josephson junction in (a) 0 and (b) π-states.

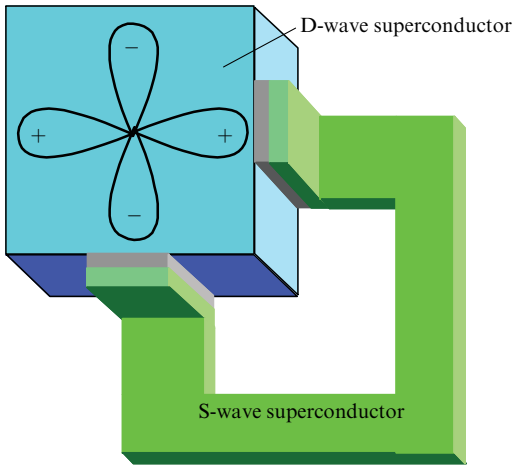

Figure 2. Schematic representation of 'corner SQUID' [11], in which an S-wave superconductor with the isotropic order parameter closes two perpendicular faces of a D-wave superconductor crystal, characterized by different signs of order parameter in two perpendicular directions of k-space.

2. Josephson π-junctions

Josephson π-junctions [10] are weakly coupled (Josephson) superconducting structures with a phase difference $\phi = \pi$ of the macroscopic wave function at their 'banks' in the ground state (i.e., in the absence of external fields and currents). As noted in the Introduction, they are characterized by an inverse current–phase relation (CPR): $I_S = I_c \sin(\phi + \pi) = -I_c \sin\phi$, i.e., a nominally 'negative' critical current $-I_c$ and a negative Josephson energy $E_\pi = -E_J \cos\phi$, where $E_J = I_c \Phi_0/(2\pi)$ and $\Phi_0 = h/2e$ is the magnetic flux quantum. The inverse CPR and coupling energy $E = E_J(1 + \cos\phi)$ in the π-junction are shown in Fig. 1b.

The inversion of the superconducting phase difference (π-state) has been actively studied in three types of Josephson structures: in an 'corner superconducting quantum interference device' ('corner SQUID' [11]) based on a closure of two perpendicular crystal faces of a high-temperature superconductor with D-wave symmetry of superconducting wave function (order parameter) using a conventional S-wave superconductor, as shown schematically in Fig. 2; in an SNS junction with a nonequilibrium electron distribution in the N barrier [3] (see Sections 4 and 5); and in a π-junction based on a Josephson SFS sandwich with an F barrier made of a weak ferromagnet [5, 7]. In the first case, the emergence of the π-state is related with the dependence of the superconducting order parameter sign on the direction in the crystal of the D-wave superconductor [11]. In the second case, it is explained by the formation of a nonequilibrium distribution of carriers in the Josephson barrier, leading to a shift of the SNS system into the Andreev conductance band with inversion of the superconducting current sign (for details, see Sections 4 and 5). In the third case, it is due to spatial oscillations (periodic sign change) of the induced superconducting order parameter in a weak ferromagnet near the S/F interface [12–14] (see [15, 16] for an overview).

The physical reason for the spatial oscillations near the SF interface is the effect on the Cooper pair (a pair of electrons with opposite spins) by the exchange field h in the ferromagnet, which leads to the emergence of a nonzero total momentum $\hbar Q$ of the Cooper pair and a continuous change Qx in the phase of the order parameter with distance from the S/F interface. Due to these oscillations, different order

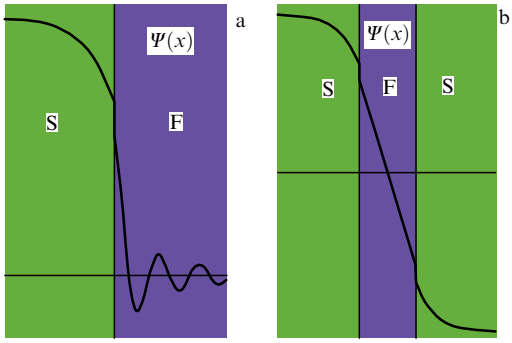

Figure 3. Alternating superconducting wave function Ψ (superconducting order parameter): (a) in SF bilayer near SF interface and (b) in SFS π-junctions.

parameter signs can arise on the two sides of the SFS sandwich when the thickness of the ferromagnetic layer is about half the oscillation period (Fig. 3), which corresponds to a change in the sign of the superconducting current and negative Josephson junction energy.

Note that, in Josephson junctions with direct conductivity (SNS, SFS junctions and superconducting bridges), in contrast to tunnel Josephson SIS junctions with a dielectric barrier (I), the current-phase relation is not purely sinusoidal, i.e., the Fourier series expansion of the corresponding 2π-periodic CPR contains noticeably higher Fourier components: $I_J = I_{c1}\sin\phi + I_{c2}\sin(2\phi) + \ldots$. At the same time, during the transition from the '0' state to the π-state (see Fig. 1), only the first Fourier component passes through zero. Thus, at the point of the '0–π' transition, the $\sin(2\phi)$ component with a π-periodic CPR (Fig. 4) may 'survive' [17].

3. Magnetic and superconducting proximity effects in Josephson S–N/F–S structures with normal metal/ferromagnet bilayer barrier

Direct electrical contact between a ferromagnet and a normal metal leads to several effects ('magnetic proximity effects'). One of them is the flow of spin-polarized electrons from F to N and the emergence of induced spin polarization in N. The contact between a ferromagnet and a normal metal leads to hybridization of electronic states and a rearrangement of the spectral densities of states in the normal metal (or superconductor) near the interface with the ferromagnet, resulting in spin splitting. This effect is atomic in scale and, from a theoretical point of view, can be described by introducing a δ-shaped Zeeman field at the interface. For thin layers of a normal metal (N) or superconductor (S) with thickness $d \ll \xi_{N,S}$ (where $\xi_{N,S}$ is the superconducting coherence length in N or S), this can be treated as the introduction of uniform effective Zeeman splitting h_{eff} in such a thin layer with amplitude $\propto d^{-1}$. The second effect is the shift of a superconducting phase difference for two bound electrons of a Cooper pair passing through or reflecting from a ferromagnetic nonsuperconducting layer. The third effect to be included in the consideration is the possibility of a Cooper pair breaking when passing through a magnet. In thin layers of a normal metal or superconductor, the last two effects can be described by introducing an effective Zeeman (exchange) field h_{eff} and an effective pair-breaking parameter Γ, respectively.

Karminskaya and Kupriyanov [18] suggested using N/F bilayers as Josephson barriers for the fabrication of planar Josephson 'magnetic' junctions. The fact is that the use of a ferromagnetic barrier (even a weak one) is only possible in SFS sandwiches, where the thickness of the F layer determines the length of the barrier. For example, the Nb–CuNi–Nb SFS sandwich, the results for which are shown in Fig. 4, had an F-layer thickness of 7 nm, although use was made of a CuNi alloy with a Curie temperature of only 60 K. To create the multiterminal structures discussed in the following sections, planar structures are needed in which a planar barrier size exceeding 50 nm is required to introduce additional quasiparticle injectors. When using S–N/F–S structures, one of which [8] is schematically shown in Fig. 5, superconducting (Andreev) transport is actually carried out through a low-resistance copper N layer due to the superconducting proximity effect, while the ferromagnetic F sublayer of a single-domain iron bar, which has a significantly higher resistance, provides an induced exchange field h_{eff} in the N layer and leads to the pair-breaking characterized by the parameter Γ.

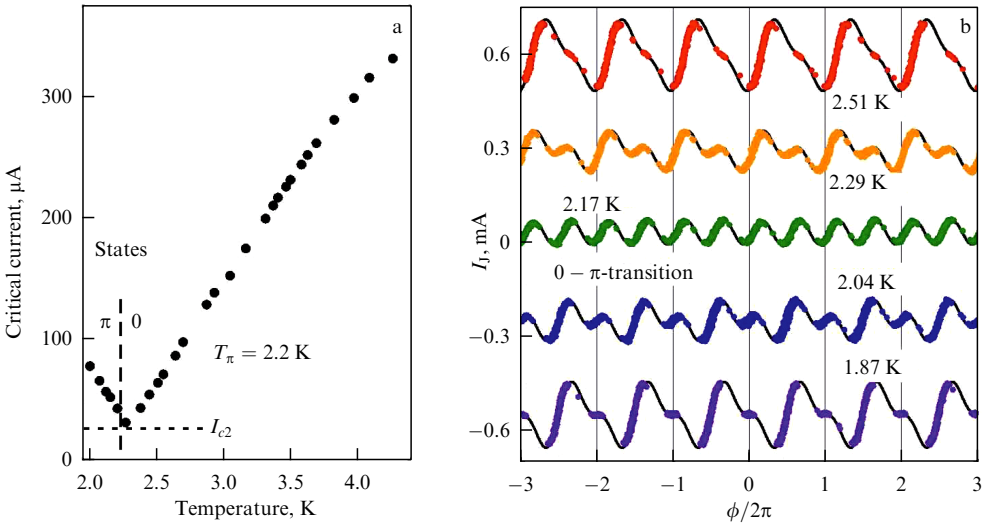

Figure 4. (a) Temperature dependence of critical current of Nb–CuNi–Nb Josephson SFS junction with transition to π-state at $T_\pi = 2.2$ K. Amplitude of second Fourier component is shown at 0–π transition point. (b) Transition from 2π-periodic CPR to π-periodic CPR near T_π.

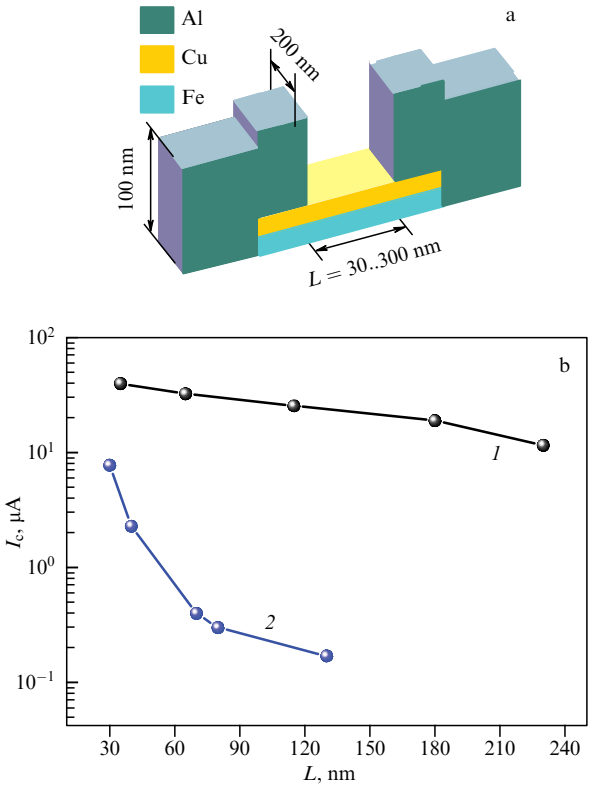

Figure 5. (a) Schematic representation of Josephson S–N/F–S structure of Al–Cu/Fe–Al. (b) Dependences of critical currents on distance between superconducting aluminum banks 'overlapping' on both sides onto N/F bilayer (curve *2*) for structure shown in panel (a) and for S–N–S structure of Al–Cu–Al with same geometry, in which F sublayer is absent (curve *1*).

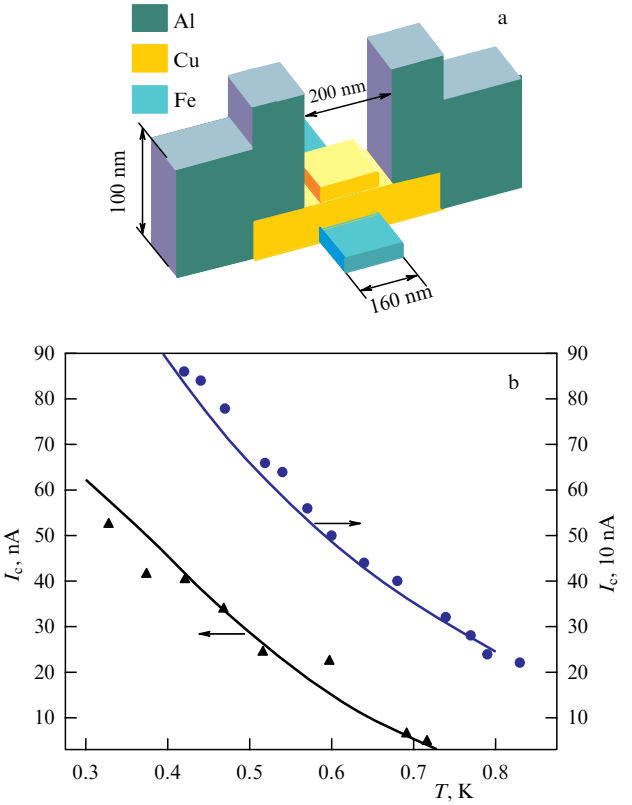

Figure 6. (a) Schematic representation of Josephson S–N/F–S structure of Al–Cu/Fe–Al. (b) Temperature dependences of critical currents for structure shown in panel (a) (lower curve) and for S–N–S structure of Al–Cu–Al with same geometry, in which F sublayer is absent (upper curve).

A comparison of the experimental dependences of critical currents on the distance between superconducting aluminum electrodes for the structure shown in Fig. 5a and for the S–N–S structure Al–Cu–Al with the same geometry, in which the F sublayer was absent, is presented in Fig. 5b [8]. One can see a significant suppression of induced superconductivity in the N barrier associated with the F-sublayer-induced h_{eff} and Γ.

A comparison of the temperature dependences of the critical current for the S–N/F–S structure with the F sublayer, schematically shown in Fig. 6a, and a similar S–N–S structure without this sublayer can be seen in Fig. 6b [9]. The solid lines represent theoretical calculations based on Usadel equations for Green's functions in the Keldysh technique [9].

A comparison of experimental and numerical results allowed us to extract the following important parameters used to fit experimental curves: induced exchange field h_{eff}, effective distance between the S electrodes [19], SN and NF interface resistances, and the pair-breaking parameter Γ related to Cooper pairs leakage into the F layer and their pair-breaking there.

The occurrence of spin polarization caused by the contact of N and F layers in S–N/F–S structures was confirmed by detecting the splitting into two spin components (↑ and ↓) of the superconducting energy gap and minigap [8] presented in Fig. 7, where the dependences of the differential resistance $\mathrm{d}V/\mathrm{d}I$ vs voltage V (for the Josephson structures represented in Figs 5a and 6a) are shown. Figure 7a shows the experimentally detected splitting of the gap singularity into two peaks, related to the difference between energy gaps for the spin up and spin down components, and Fig. 7c demonstrates the spin splitting of the superconducting minigap induced in the N layer.

To ensure that the observed splitting is indeed related to spin polarization induced in the copper N layer due to the magnetic proximity effect with the single-domain F layer, magnetic force microscopy was used to verify that the easy magnetic axis lies along the iron sublayer and that it can be remagnetized by an external magnetic field, which is perpendicular to the easy magnetic axis in the plane of the N/F bilayer, as shown in Fig. 7b. Measurement of the anisotropic magnetoresistance of a single iron layer with the corresponding dimensions of 700×200 nm^2, used in the S–N/F–S structure the splitting $\Delta V(H)$ for which is shown in Figs 7d and 7c, demonstrated that the greatest magnetic disorder is reached at $H = H_{\text{coercive}} \approx 300$ Oe. One can see that the value ΔV is minimal at this magnetic field and then increases during remagnetization in the perpendicular direction.

4. Andreev current-transport in superconductor–normal metal–superconductor in the diffusive limit. Effect of induced exchange field

In the Introduction, we discussed the fact that coherent supercurrent transport through the N barrier in the SNS junction in the clean (ballistic) limit occurs due to Andreev

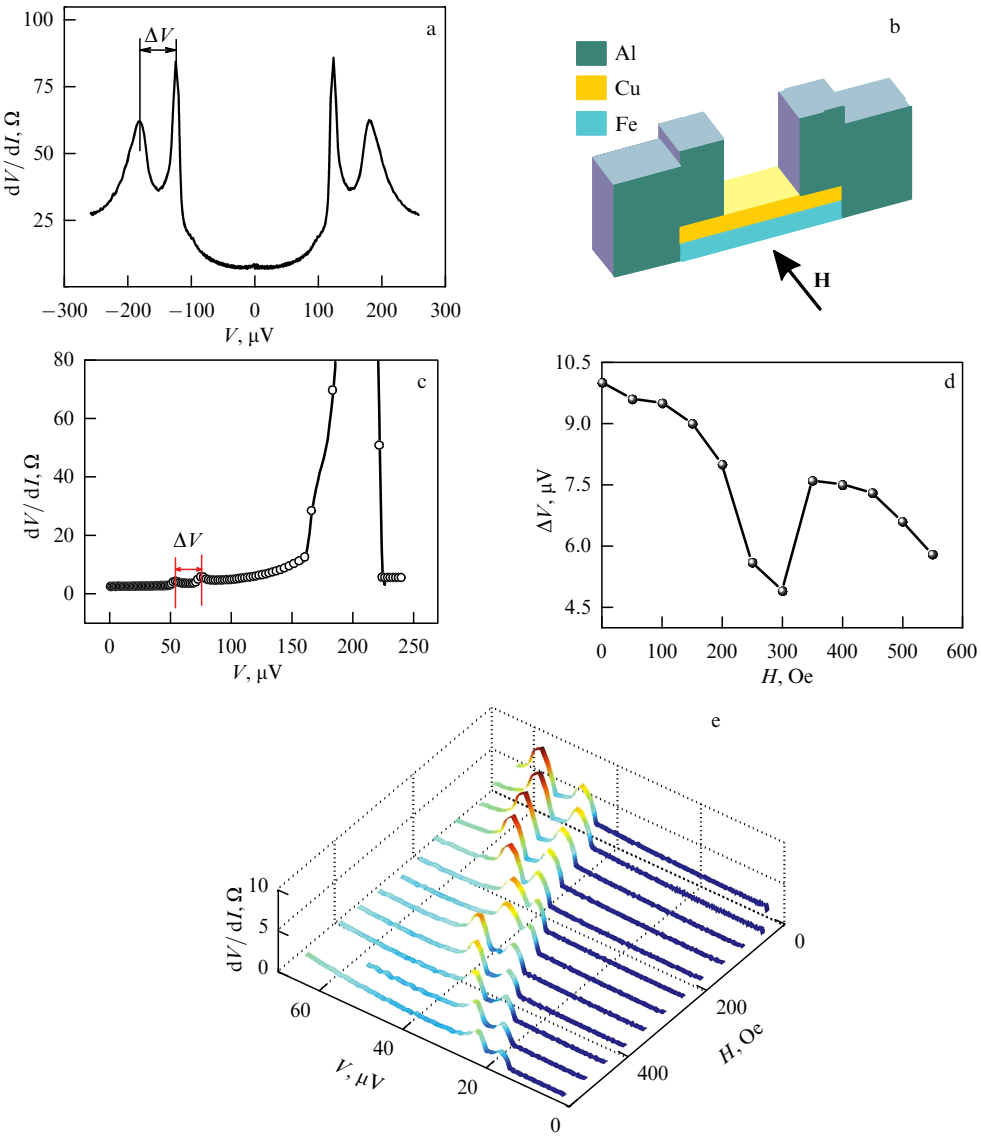

Figure 7. (a) Splitting of the gap singularity into two spin components. (b) 'Demagnetization' of F layer by field perpendicular to easy axis. (c) Spin splitting of superconducting minigap induced in N layer. (d) Dependence of spin splitting of minigap ΔV on magnetic field applied in plane of N/F bilayer perpendicular to magnetic easy axis of F sublayer, as shown in panel (b). (e) Characteristics of differential resistance $dV/dI(V)$ as a function of external magnetic field H used to extract splitting ΔV shown in panel (d).

reflection from two NS interfaces and the emergence of pairs of Andreev levels that carry superconducting currents in opposite directions. In the diffusive limit, the levels smear into energy bands, and coherent electron transport is determined by the supercurrent-carrying density of states (SCDOS), the simplest of which for the structure [20] shown in Fig. 8a is presented in Fig. 8b. One can see that, in the case of the SNS structure, SCDOS has only two bands with different signs, responsible for two opposite directions of supercurrent; i.e., only one '0–π' transition with inversion of the current–phase relation is possible. This transition, first observed in [3], is shown in Fig. 9.

In fact, Baselmans et al. [3, 20] measured the current–voltage curves $V_{SNS}(I_{SNS})$ between the two S banks of the SNS junction (Fig. 9b), which are shown in the inset to Fig. 9a. These curves make it possible to extract only the absolute values of the critical superconducting current I_c. However, Baselmans et al. [3] placed the values of I_c for $V_{control} > 0.5$ mV in the negative region of the plot (Fig. 9a), assuming that they correspond to the inverted current–phase relation $I_S = I_c \sin(\phi + \pi) = -I_c \sin\phi$.

The SCDOS band structure (more precisely, the energy dependence $\mathrm{Im}\,(J(\varepsilon))$, as shown in Fig. 8b, is calculated based on the microscopic theory of quasi-classical Green's functions [21, 22]. The critical current I_c of the SNS junction in the case of a nonequilibrium quasiparticle distribution function $f(\varepsilon)$ is calculated using the formula

$$I_c = \frac{1}{R_n}\int_{-\infty}^{\infty} d\varepsilon\,[1 - 2f(\varepsilon)]\,\mathrm{Im}\left[J\left(\varepsilon, \phi = \frac{\pi}{2}\right)\right], \qquad (1)$$

where R_n is the normal resistance of the SNS junction, $1 - 2f(\varepsilon)$ is the distribution function for superconducting carriers, and $\mathrm{Im}\,[J(\varepsilon, \phi)]$ is the SCDOS.

As noted in the Introduction, Golikova et al. [9] investigated a more complex S–N/F–S structure (Fig. 6a),

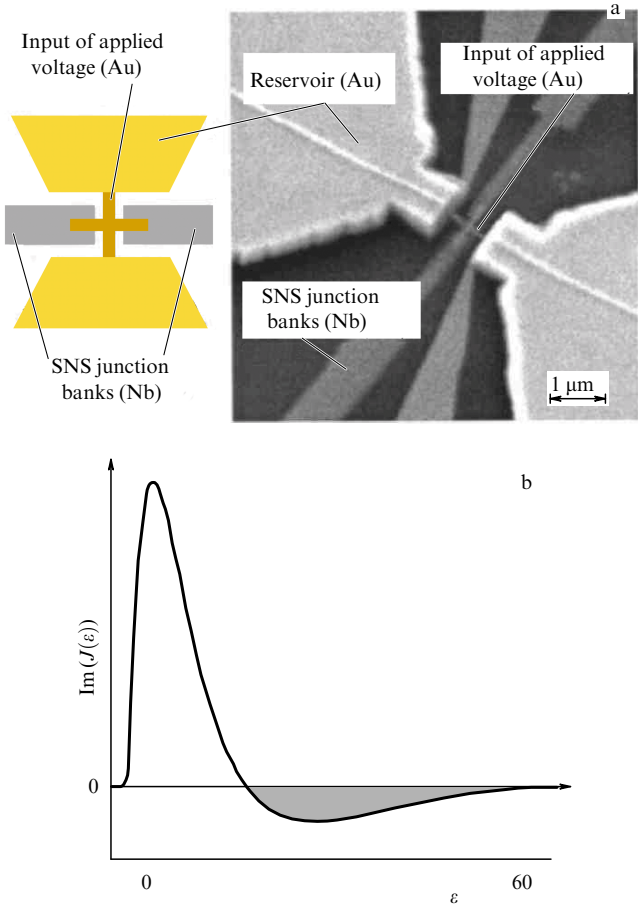

Figure 8. (a) Schematic representation and micrograph of SNS structure used in experiment [20]. (b) Two-band SCDOS for this structure. Energy ε is normalized to Thouless energy $E_{\rm th}$.

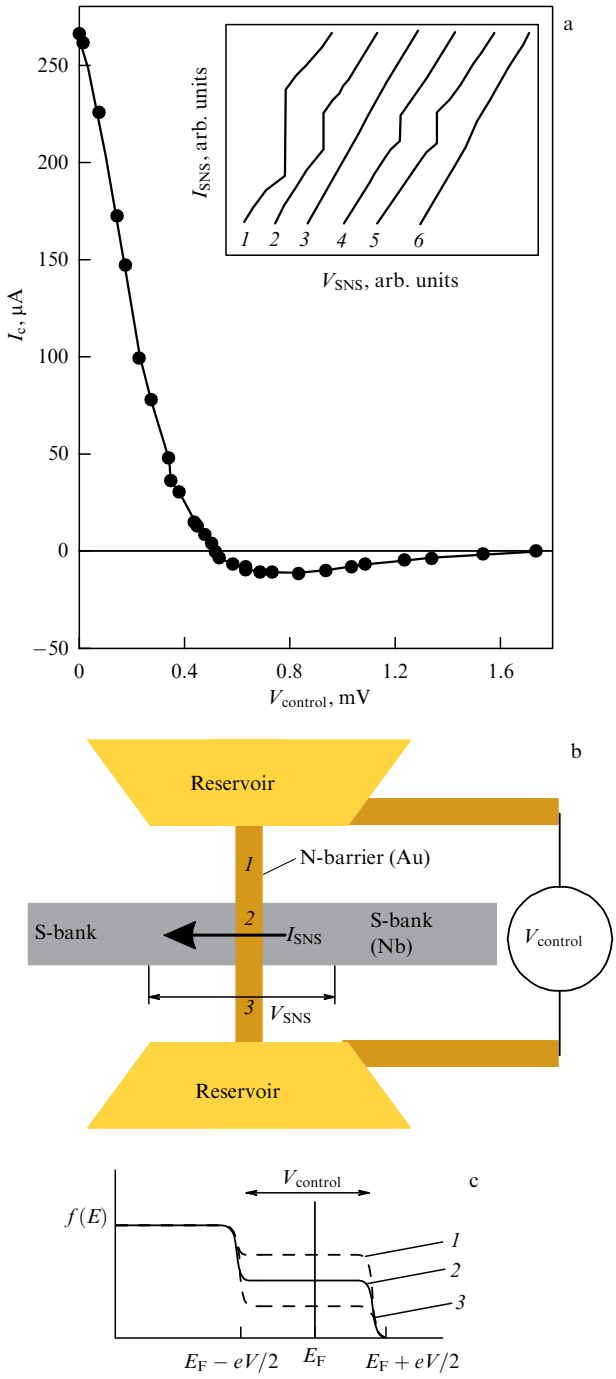

Figure 9. (a) Dependence of critical current I_c of Nb–Au–Nb SNS junction on control voltage $V_{\rm control}$; inset shows current-voltage curves from which I_c values are extracted. (b) Schematic representation of measured structure [3] with geometry of current setting, control voltage $V_{\rm control}$, and measured voltage $V_{\rm SNS}$. (c) Step nonequilibrium distribution functions arising in N barrier upon application of voltage $V_{\rm control}$ between electron reservoirs (extensions); numbers *1*, *2*, and *3* mark three step distributions at corresponding locations along N barrier.

for which the SCDOS calculations are shown in Fig. 10d. Figure 10a shows the SCDOS for the studied structure, taking into account the actual transparency of the SN interfaces and the length of the N layer, but without the induced $h_{\rm eff}$ and Γ. Figure 10b demonstrates a change in the SCDOS when a small induced exchange field, $h = 0.2\Delta$, appears (where Δ is the energy gap in the S banks). One can see that, in the energy range smaller in magnitude than the effective exchange field, SCDOS splitting occurs, and, at $\varepsilon > 0$, a peak of the opposite sign appears, which provides a possibility of an additional 0–π transition when controlling the distribution function. Figure 10c shows a change in the SCDOS at $h = 1.41\Delta$, obtained from the fit of experimental data. There are still two crossing (at $\varepsilon > 0$) with the SCDOS sign changes. Finally, Fig. 10d demonstrates the pair-breaking parameter Γ taken into account, i.e., the leakage of Cooper pairs into the iron layer with their subsequent breaking in this layer. One can see that the appearance of unpairing, Γ, leads to the smearing of the SCDOS, but does not change the situation qualitatively.

When fitting the experimental data, Golikova et al. [9] extracted the following structure parameters: transparency of the SN interfaces, effective $h_{\rm eff}$ and Γ induced in the N layer by the proximity effect with the iron sublayer, the system's sensitivity coefficient to overheating due to the injection current, and the effective distance between the S electrodes. The last is worth noting separately, since this distance does not coincide with the actual physical distance L between the S banks but exceeds it (Figs 5a and 6a). The reason for this is the complex geometry of the junction, where the superconducting layers overlap the normal layer from above and the supercurrent does not flow along the minimum distance between the superconductors [19].

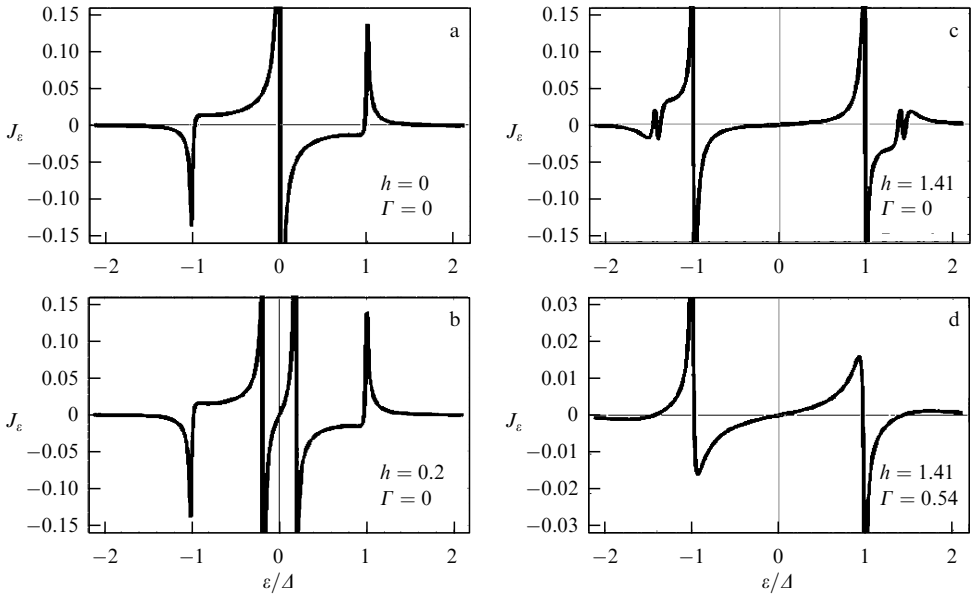

Figure 10. Evolution of SCDOS with addition of a ferromagnetic sublayer to Josephson barrier of SNS junction, causing appearance of induced exchange field h in N barrier. (a) Two-band SCDOS for SNS junction without ferromagnetic (F) iron sublayer with geometry of copper (N) barrier and aluminum (S) banks corresponding to Fig. 6a. (b) SCDOS for similar structure with F sublayer, providing a small value of induced exchange field $h = 0.2$ in absence of leakage of superconducting carriers into F sublayer ($\Gamma = 0$). (c) SCDOS for structure with F sublayer at $h = 1.41$ (exchange energy corresponds to the experiment and exceeds energy gap Δ in S banks), $\Gamma = 0$. (d) SCDOS calculation based on geometry of the structure (Fig. 6a) and parameters $h = 1.41$ and $\Gamma = 0.54$, obtained from comparison of experimental and numerical results of $I_c(T)$ (Fig. 6b).

5. Effect of nonequilibrium quasiparticle injection on properties of Josephson superconductor–normal metal–superconductor junctions. Features of distribution function upon injection of spin-polarized carriers into N barrier

To transfer the Josephson system to a higher energy band of the SCDOS, Baselmans et al. [3, 20] used control voltage V_{control} (more precisely, energy $\varepsilon = eV_{\text{control}}$) applied between the normal-metal reservoirs shown in Fig. 9b. The presence of the reservoir extensions allows to create an electronic distribution in the form of a sharp step in the Josephson N barrier. Increasing the control voltage V_{control} makes it possible to shift this distribution step along the energy axis ε [the horizontal axis in the SCDOS plots (Fig. 11)] and move it along the Andreev bands. Figure 11 shows on the left that the 'smeared' ('thermal') distribution (as opposed to the step distribution) 'sweeps' both Andreev bands and does not provide inversion of the current–phase relation, although it can modify it. This situation was observed, for example, by Fuechsle et al. [23], who studied a nonequilibrium distribution function under microwave irradiation of the SNS junction.

To describe theoretically the nonequilibrium distribution function arising in the structure used for the experiment [9] (its cross section along the F sublayer is shown in Fig. 12a), a simulation was performed for a simplified structure shown in Fig. 12b (i.e., for a F/N/F spin valve with parallel magnetizations). Such a replacement is quite reasonable, since the entire current I_{inj}, set by the control voltage V_{control} between the reservoirs, actually flows through the N layer (shown in Fig. 12a), since the resistance of the copper layer (with $\rho_N = 4.5$ μΩ cm and a thickness of 60 nm) is much lower

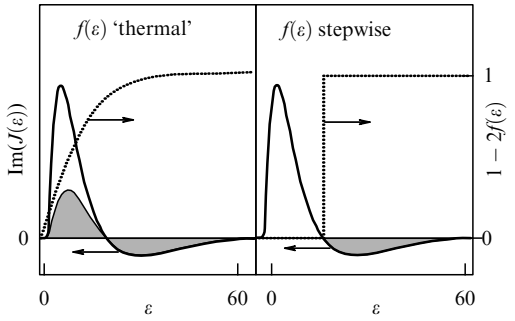

Figure 11. SCDOS for SNS junction with 'smeared' ('thermal') and stepwise distribution of superconducting carriers, $1-2f(\varepsilon)$.

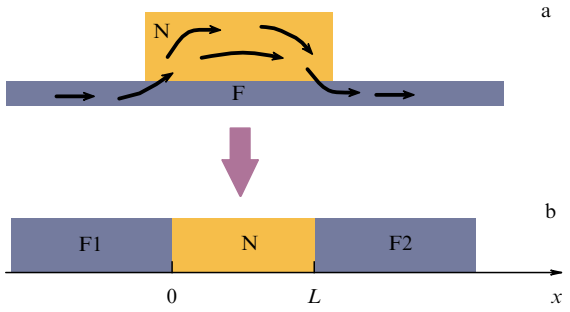

Figure 12. (a) Schematic cross-section along F sublayer of real structure used in [9] (Fig. 6a). (b) Schematic representation of simplified structure used for simulation.

than that of the iron sublayer (with $\rho_F = 70$ μΩ cm and a thickness of 10 nm).

In the case of injection of spin-polarized carriers, the distribution functions of the two spin subbands $\varphi_{\uparrow,\downarrow}$ become different in the N layer (Fig. 13).

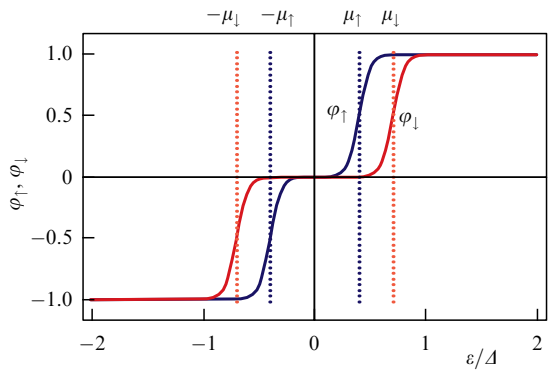

Figure 13. Distribution functions $\varphi_{\uparrow,\downarrow}$ for two spin subbands calculated in ideal ('nonthermalized') case.

Here, the expression for the Josephson current in terms of the SCDOS and the nonequilibrium distribution function is slightly modified compared to formula (1):

$$j_c = \frac{d}{8eR_{NF}} \int_{-\infty}^{\infty} d\varepsilon \sum_{\sigma} \left(\varphi_\sigma(\varepsilon) + \tilde{\varphi}_\sigma(\varepsilon)\right) \mathrm{Im}\left[J_{\varepsilon,\sigma}\right], \qquad (2)$$

where R_{NF} is the normal resistance of the bilayer N/F barrier, $\varphi_\sigma(\varepsilon) + \tilde{\varphi}_\sigma(\varepsilon)$ is the effective quasiparticle distribution, and $\mathrm{Im}\left[J_{\varepsilon,\sigma}\right]$ is the SCDOS for a given spin subband σ. Golikova et al. [9] showed that, for the considered configuration of a spin valve with parallel magnetizations of the layers, these functions must be antisymmetric with respect to the electron energy ε. Their characteristic shape is shown in Fig. 13.

To understand the physical meaning of the imbalance created by passing current through the parallel spin valve, let us consider possible physically different ways of constructing a nonequilibrium distribution of quasiparticles in an arbitrary Fermi liquid system. Any nonequilibrium distribution of quasiparticles can be decomposed into four so-called nonequilibrium modes describing physically different ways of creating a nonequilibrium distribution of quasiparticles in the system [24, 25]. In the literature, they are usually denoted as ϕ_L, ϕ_T, $\phi_{L,3}$, and $\phi_{T,3}$. The complete nonequilibrium distribution function is the sum of all these modes and the equilibrium value $1 - 2f_0(\varepsilon)$, where $f_0(\varepsilon)$ is the Fermi function.

The physical meaning of individual nonequilibrium modes is schematically explained in Fig. 14. Figures 14a and 14b depict the equilibrium Fermi distribution of quasiparticles in the electron subsystem corresponding to a given temperature T. In Fig. 14a, the equilibrium distribution is represented in terms of Bogoliubov quasiparticles in a superconductor. Black dots represent electron excitations, circles show hole excitations, and gray dots are electron–hole excitations near the edge of the gap. The electron and hole branches of the excitation spectrum are populated equally. The spin branches corresponding to spins up and spins down are also populated equally (compare here and further the right and left columns on the left in Fig. 14). Plot on the right in Fig. 14b shows the same distribution in terms of the electron distribution $\varphi(\varepsilon) = [1 - 2f(\varepsilon)]$, which is used in the theoretical description in terms of Usadel equations and the expression for the current. The physical meaning of $\varphi(\varepsilon)$ is the difference between the hole and electron distribution functions $f_h(\varepsilon) - f_e(\varepsilon)$, i.e., φ differs from ± 1 at the energies where any quasiparticles are present.

ϕ_L is called the energy mode and describes any spin-independent and symmetric (on the number of electron-like and hole-like excitations) deviations of the distribution in the electron subsystem from the Fermi distribution corresponding to the ambient temperature (Figs 14c and 14d). For example, this mode describes the overheating of the electron subsystem or the nonthermalized two-step distribution of quasiparticles shown in Fig. 9c.

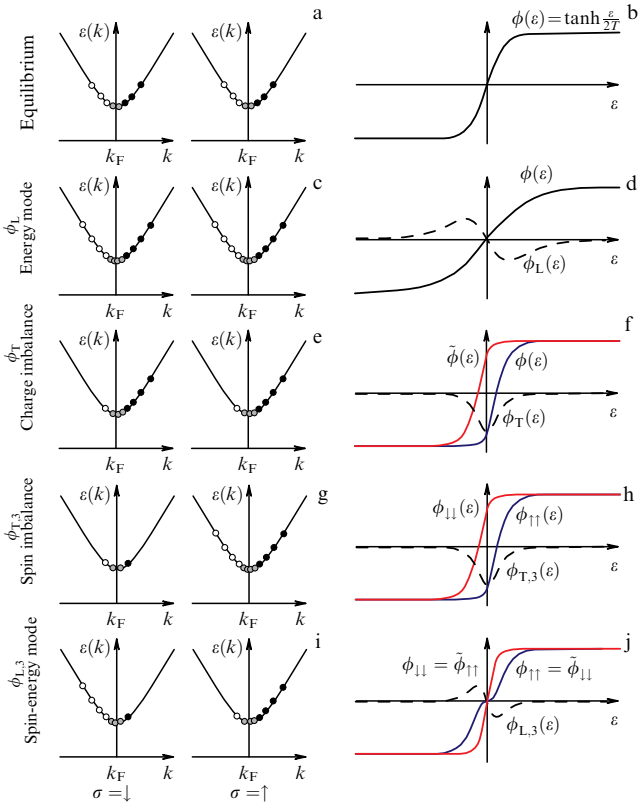

Figure 14. Various nonequilibrium modes: (a, c, e, g, i) in terms of Bogoliubov quasiparticles and (b, d, f, h, j) in terms of electron distribution included in the Usadel equation. Black dots are electron excitations, circles are hole excitations, and gray dots are electron-hole excitations near edge of gap. For further description of modes, see text. (Figure borrowed from [26].)

ϕ_T is the well-known charge imbalance. It corresponds to different numbers of electron-like and hole-like excitations of the quasiparticle spectrum (Figs 14e and 14f). The charge imbalance in Fig. 14e is visible as different numbers of electron and hole excitations. In Fig. 14f, it manifests itself as an opposite energy shift of the electron $\varphi(\varepsilon)$ and hole $\tilde{\varphi}(\varepsilon)$ distribution functions, which are shown in blue and red, respectively. That is, this mode corresponds to the appearance of a nonzero quasiparticle charge in the system and can be obtained from the equilibrium Fermi distribution without redistribution of excitations across energy levels. In this case, ϕ_T, like ϕ_L, does not depend on the spin of the quasiparticle.

The mode $\phi_{T,3}$ is the spin imbalance. It is shown in Figs 14g and 14h. In this mode, an equal number of electron-like and hole-like quasiparticles are excited, but the number of excitations is different for spins up and spins down. Thus, a nonzero total quasiparticle spin appears in the system.

$\phi_{L,3}$ is called the spin-energy mode in the literature [24, 25]. It also results in a spin-split distribution of quasiparticles, but does not lead to the accumulation of total spin. Although, separately, quasiparticles with spins up and down in this mode have a charge imbalance (Fig. 14i), the

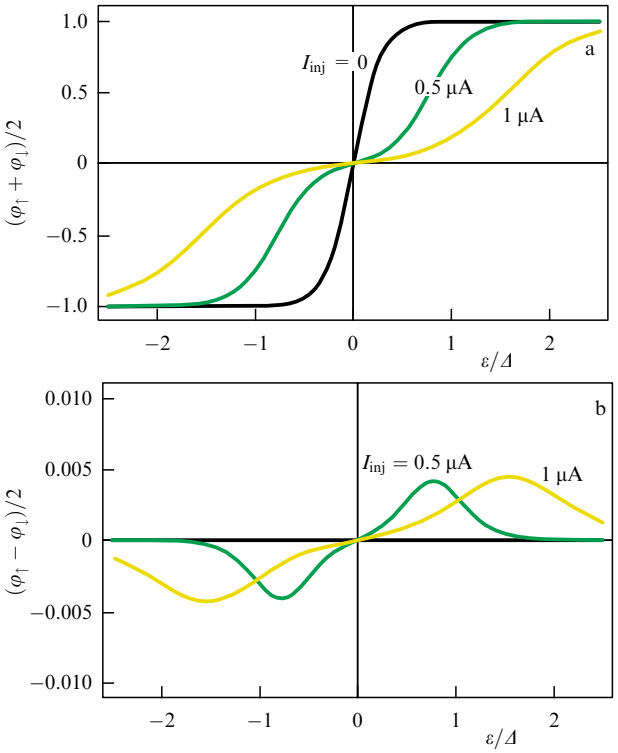

Figure 15. Nonequilibrium quasiparticle distributions (a) $f_L = 1/2\,(\varphi_\uparrow + \varphi_\downarrow)$ and (b) $f_{L,3} = 1/2\,(\varphi_\uparrow - \varphi_\downarrow)$, calculated for parameters of experiment [9].

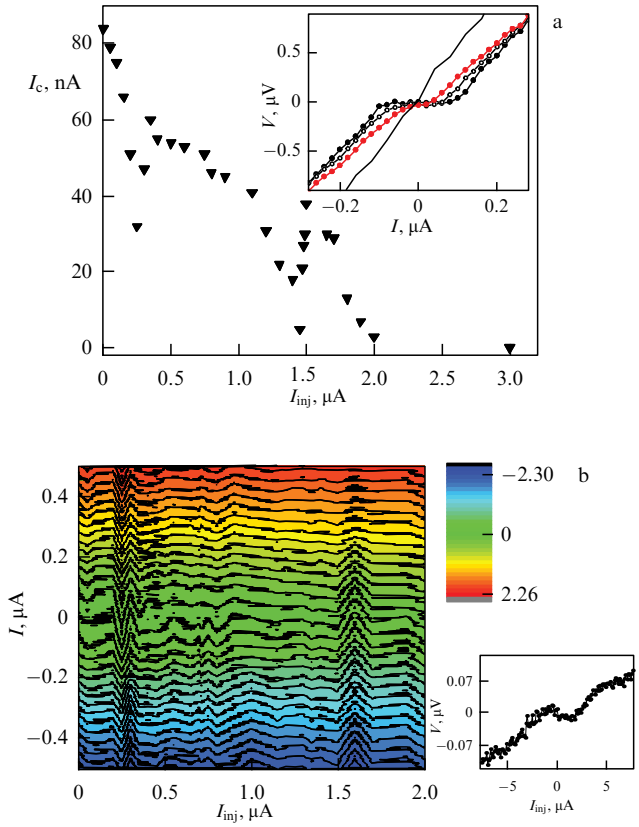

Figure 16. (a) Critical current I_c for Josephson S–N/F–S structure of Al–Cu/Fe–Al as a function of injection current I_{inj} into Cu/Fe barrier at $T = 0.3$ K. Inset shows current-voltage curves along Josephson structure for different I_{inj}: black dots for 0, gray dots for 1 μA, and red dots for 1.7 μA. (b) Three-dimensional representation of current–voltage curves as a function of injection current.

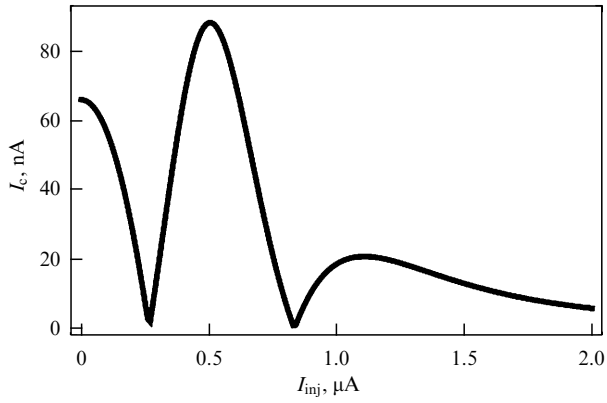

Figure 17. Critical current I_c for S–N/F–S structure, calculated using SCDOS presented in Fig. 10d and distribution function shown in Fig. 15.

charge imbalance summed over both spins in this system is zero.

The modes ϕ_L and $\phi_{L,3}$ are always odd in energy, while the modes ϕ_T and $\phi_{T,3}$ are even. At the same time, the spin-summed part of the SCDOS is odd in ε, and the spin-antisymmetric part of the SCDOS is even in ε. Therefore, it can be shown that in the calculation of the critical current the energy modes ϕ_L and $\phi_{L,3}$ interact only with the spin-averaged part of the SCDOS, the charge mode ϕ_T within the framework of formula (2) does not contribute to the critical current, and the spin imbalance $\phi_{T,3}$ senses only the spin-antisymmetric part of the SCDOS [27, 28].

Referring again to Fig. 13, one can understand, based on the given classification of nonequilibrium modes, that an electric current passing through the spin valve in the parallel configuration results in some combination of energy and spin-energy nonequilibrium modes. For this type of nonequilibrium distribution, the total charge and spin of the quasiparticles are zero. Golikova et al. [9] estimated the contributions of the energy and spin-energy nonequilibrium modes to the nonequilibrium distribution created by the quasiparticle injection current I_{inj} through the F layer. The results of the calculations performed for the parameters of experiment [9] are shown in Fig. 15. The difference between electrochemical potentials $\mu_\downarrow - \mu_\uparrow = (\alpha_\downarrow - \alpha_\uparrow)I_{inj}$ turned out to be quite small, since $(\alpha_\downarrow - \alpha_\uparrow)$ is limited by the comparatively low polarization in iron, which further decreases after passing into the N layer through the F/N interface. As a result, the main contribution to nonequilibrium was made by the energy mode (Fig. 15a), and the calculated spin-energy mode $f_{L,3}$, shown in Fig. 15b, turned out to be negligibly small.

Using the parameters obtained for the case of [9], we used formula (2) to calculate the critical current density of the S–N/F–S structure. In the case of an antisymmetric energy distribution, it can be shown that the effective distribution function, which is included in the formula for the current (2), has the form $\varphi_\sigma(\varepsilon) + \tilde{\varphi}_\sigma(\varepsilon) = \varphi_\uparrow + \varphi_\downarrow$, i.e., is determined only by the energy nonequilibrium mode. The energy nonequilibrium mode φ_L (Fig. 15a) retained the step shape of the distribution function (although 'smeared' by the heating of the interlayer region by the injection current), at least up to $I_{inj} = 2$ μA. This was sufficient to observe the manifestation of the third 'Andreev' band, discovered in the calculation (see Fig. 10) and associated with the spin splitting of SCDOS.

The calculation result shown in Fig. 17 qualitatively repeats the experimental dependence $I_c(I_{inj})$, presented in Fig. 16a, which indicates the observation of a double 0–π–0 transition, but there is no quantitative correspondence due to the complex geometry of the real S–N/F–S structure.

6. Conclusions

Coherent current transport through a nonsuperconducting barrier, first predicted by B.D. Josephson [29] for a tunnel SIS junction with a dielectric (I) barrier, has a much more complex and interesting nature in the case of Josephson junctions with barriers made of normal metals (SNS junctions) and ferromagnets (SFS junctions). The understanding of superconducting transport in these Josephson systems was significantly influenced by the discovery of two amazing phenomena: Andreev reflection and the emergence of inhomogeneous 'alternating' superconductivity under the influence of Zeeman (spin) splitting. The description of these phenomena significantly expanded the initial ideas about the Josephson effect and the superconducting (Cooper) electron pair according to Bardeen, Cooper, and Schrieffer [30]. First of all, in 1964, A.F. Andreev [1] explained coherent current transport across a single NS interface by 'Andreev reflection,' and, in 1969, I.O. Kulik [2] showed that Andreev reflection leads to the emergence of a system of levels ('Andreev levels') responsible for superconducting transport through SNS structures. Later, it was shown that changes in the energy and magnetic (spin) state of electrons in the Josephson barrier can significantly change the relation (predicted by B.D. Josephson), $I_S = I_c \sin\varphi$, between the superconducting current I_S and the phase difference φ at the Josephson junction. The current-phase relation changes most dramatically during the transition to the 'π-state,' with an inversion of the phase difference: from $I_S = I_c \sin\varphi$ to $I_S = I_c \sin(\varphi + \pi) = -I_c \sin\varphi$. This transition from the ordinary ('0 state') to the π-state occurs in the equilibrium case in the SFS junction in connection with the interaction of Cooper pairs (or, in the 'Andreev' terms, coupled electron-hole pairs) penetrating into the ferromagnet with the exchange field h in it [12, 13] due to the emergence of a nonzero total momentum $\hbar Q$ and a phase shift of the order parameter $Qd \propto \pi$ over the thickness of the ferromagnetic barrier d. Such an inhomogeneous 'alternating' superconductivity (LOFF-state) in the presence of an exchange or externally applied magnetic field, caused by Zeeman splitting of the spin-degenerate state of the BCS pair, was first predicted in 1964 by Larkin–Ovchinnikov and Fulde–Ferrel [31, 32]. Detailed experiments with the observation and study of 0–π transitions in SFS sandwiches were performed in papers [5, 7, 17] and others with the participation of the authors of the present review.

In 1999, Bazelmans et al. [3, 20] showed experimentally that the transition to the π-state in the Josephson SNS junction can be induced by a nonequilibrium electron energy distribution in the N barrier, specified by the voltage V across the N layer. The applied energy eV, comparable to the energy interval between neighboring Andreev levels (bands in the diffusive case), transfers the SNS system to a higher level (band), responsible for the superconducting current in the opposite direction, which corresponds to a shift of the current–phase relation by π: from $I_S = I_c \sin\varphi$ to $I_S = I_c \sin(\varphi + \pi) = -I_c \sin\varphi$. As was shown in [21, 22], supercurrent in Josephson structures with normal–metal barriers and diffusive electron transport is determined by the 'supercurrent-carrying density of states,' which in the simplest case of an SNS junction has only two bands responsible for the transport of superconducting currents of opposite signs.

In the discussed studies [8, 9] by our group, the structure of the Andreev current-carrying states was modified due to the presence of electric contact between the copper N layer in the Josephson barrier and the ferromagnetic iron F sublayer. The induced exchange field due to spin diffusion from the F to the N layer allowed the structure of the supercurrent-carrying density of states in the N/F barrier to be more complicated by increasing the number of bands carrying superconducting currents of opposite signs. An increase in the injection current into the Josephson barrier made it possible to sequentially pass through three Andreev current-carrying states by means of shifts of the step of nonequilibrium energy distribution and observe two transitions: the first from the usual (0 state) to the π-state and the second back from the π to the 0 state. Thus, it was shown experimentally and theoretically that spin diffusion and injection of unpolarized and spin-polarized carriers into the Josephson barrier allows one to significantly change the coherent Andreev current transport in Josephson SNS structures.

At the same time, many possibilities remain unexplored both from the point of SCDOS engineering and nonequilibrium control, primarily in terms of their experimental implementation. The creation of spin-split SCDOS in normal metal–ferromagnetic insulator bilayers seems interesting, but has not yet been implemented. Unlike the bilayers with a ferromagnetic metal considered in this review, there is assumed to be an almost complete absence of the depairing factor Γ due to the absence of pair breaking in the ferromagnetic insulator. The absence of Γ should lead to more pronounced spin-dependent SCDOS and more effective control of Josephson 0–π transitions. To date, only ferromagnetic insulator–superconductor bilayers have been experimentally studied, in which well-defined spin splitting of the local density of states was observed at a very small value of Γ [24, 25]. Also, control of Josephson junctions using spin imbalance has not yet been implemented [27, 28]. This requires a spin-asymmetric (in contrast to the symmetric one in [9]) injection of spin-polarized current from ferromagnets into the weak link region.

References

1. Andreev A F *Sov. Phys. JETP* **19** 1228 (1964); *Zh. Eksp. Teor. Fiz.* **46** 1823 (1964)
2. Kulik I O *Sov. Phys. JETP* **30** 944 (1970); *Zh. Eksp. Teor. Fiz.* **57** 1745 (1969)
3. Baselmans J J A et al. *Nature* **397** 43 (1999)
4. Ryazanov V V *Phys. Usp.* **42** 825 (1999); *Usp. Fiz. Nauk* **169** 920 (1999)
5. Ryazanov V V et al. *Phys. Rev. Lett.* **86** 2427 (2001)
6. Ryazanov V V et al. *Phys. Usp.* **47** 732 (2004); *Usp. Fiz. Nauk* **174** 795 (2004)
7. Oboznov V A et al. *Phys. Rev. Lett.* **96** 197003 (2006)
8. Golikova T E et al. *Phys. Rev. B* **86** 064416 (2012)
9. Golikova T E et al. *Supercond. Sci. Technol.* **34** 095001 (2021)
10. Bulaevskii L N, Kuzii V V, Sobyanin A A *JETP Lett.* **25** 290 (1977); *Pis'ma Zh. Eksp. Teor. Fiz.* **25** 314 (1977)
11. Wollman D A et al. *Phys. Rev. Lett.* **71** 2134 (1993)
12. Buzdin A I, Bulaevskii L N, Panyukov S V *JETP Lett.* **35** 178 (1982); *Pis'ma Zh. Eksp. Teor. Fiz.* **35** 147 (1982)
13. Buzdin A I, Bujicic B, Kupriyanov M Yu *Sov. Phys. JETP* **74** 124 (1992); *Zh. Eksp. Teor. Fiz.* **101** 231 (1992)
14. Izyumov Yu A, Proshin Yu N, Khusainov M G *Phys. Usp.* **45** 109 (2002); *Usp. Fiz. Nauk* **172** 113 (2002)

15. Buzdin A I *Rev. Mod. Phys.* **77** 935 (2005)
16. Mel'nikov A S et al. *Phys. Usp.* **65** 1248 (2022); *Usp. Fiz. Nauk* **192** 1339 (2022)
17. Stoutimore M J A et al. *Phys. Rev. Lett.* **121** 177702 (2018)
18. Karminskaya T Yu, Kupriyanov M Yu *JETP Lett.* **85** 286 (2007); *Pis'ma Zh. Eksp. Teor. Fiz.* **85** 343 (2007)
19. Bakurskiy S et al. *Mesosci. Nanotechnol.* **1** (1) 01003 (2024)
20. Baselmans J J A, van Wees B J, Klapwijk T M *Phys. Rev. B* **63** 094504 (2001)
21. Volkov A F *Phys. Rev. Lett.* **74** 4730 (1995)
22. Wilhelm F K, Schön G, Zaikin A D *Phys. Rev. Lett.* **81** 1682 (1998)
23. Fuechsle M et al. *Phys. Rev. Lett.* **102** 127001 (2009)
24. Bergeret F S et al. *Rev. Mod. Phys.* **90** 041001 (2018)
25. Heikkilä T T et al. *Prog. Surf. Sci.* **94** 100540 (2019)
26. Bobkova I V, Doctoral Thesis in Phys. and Math. (Chernogolovka: Osipyan Institute of Solid State Physics RAS, 2023)
27. Bobkov A M, Bobkova I V *Phys. Rev. B* **84** 054533 (2011)
28. Bobkova I V, Bobkov A M *Phys. Rev. B* **82** 024515 (2010)
29. Josephson B D *Phys. Lett.* **1** 251 (1962)
30. Bardeen J, Cooper L N, Schrieffer J R *Phys. Rev.* **108** 1175 (1957)
31. Larkin A I, Ovchinnikov Yu N *Sov. Phys. JETP* **20** 762 (1965); *Zh. Eksp. Teor. Fiz.* **47** 1136 (1964)
32. Fulde P, Ferrell R A *Phys. Rev.* **135** A550 (1964)